

MDSGen: FAST AND EFFICIENT MASKED DIFFUSION TEMPORAL-AWARE TRANSFORMERS FOR OPEN-DOMAIN SOUND GENERATION

Trung X. Pham*, Tri Ton*, Chang D. Yoo

Korea Advanced Institute of Science and Technology (KAIST)

{trungpx, trith, cd.yoo}@kaist.ac.kr

ABSTRACT

We introduce `MDSGen`, a novel framework for vision-guided open-domain sound generation optimized for model parameter size, memory consumption, and inference speed. This framework incorporates two key innovations: (1) a redundant video feature removal module that filters out unnecessary visual information, and (2) a temporal-aware masking strategy that leverages temporal context for enhanced audio generation accuracy. In contrast to existing resource-heavy Unet-based models, `MDSGen` employs denoising masked diffusion transformers, facilitating efficient generation without reliance on pre-trained diffusion models. Evaluated on the benchmark VGGSound dataset, our smallest model (5M parameters) achieves 97.9% alignment accuracy, using $172\times$ fewer parameters, 371% less memory, and offering $36\times$ faster inference than the current 860M-parameter state-of-the-art model (93.9% accuracy). The larger model (131M parameters) reaches nearly 99% accuracy while requiring $6.5\times$ fewer parameters. These results highlight the scalability and effectiveness of our approach.

1 INTRODUCTION

Vision-guided audio generation has gained significant attention due to its crucial role in Foley sound synthesis for the video and film production industry (Ament, 2014). This paper focuses on Video-to-Audio (V2A) generation, a key task not only for adding realistic sound to silent videos created by emerging text-to-video models (Blattmann et al., 2023; Khachatryan et al., 2023; Huang et al., 2024; Ouyang et al., 2024) but also for enhancing practical applications in professional video production. Sound generation is essential for creating immersive experiences and achieving seamless audio-visual synchronization. However, achieving both semantic alignment and temporal synchronization in V2A remains a significant challenge. Previous approaches, such as GAN-based methods (Chen et al., 2020b) and Transformer-based autoregressive models (Iashin & Rahtu, 2021), have struggled with synchronizing audio to content while maintaining relevance. Diff-Foley (Luo et al., 2023) improved this by employing contrastive learning for video-audio alignment and leveraging diffusion models, achieving impressive sound quality. Other methods like See and Hear (Xing et al., 2024) and FoleyCrater (Zhang et al., 2024) utilize large pre-trained models for high-quality audio generation. However, these models rely on hundreds of millions of parameters. In contrast, our work demonstrates that a much smaller model can deliver high performance (see Fig. 1). Most

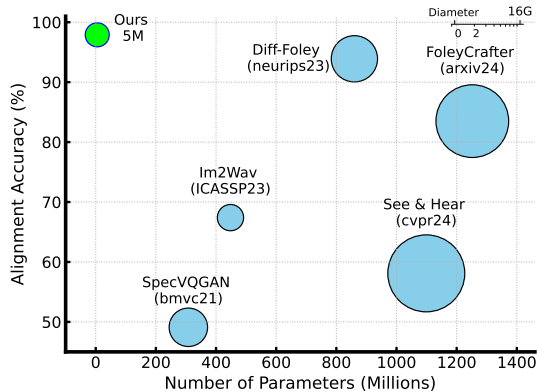


Figure 1: **Alignment Score.** Comparison with SOTA audio generation methods on the VGGSound test set. The diameter of each circle represents the memory usage during inference.

*Equal Contribution

existing approaches rely on Unet architectures, which present scalability limitations. Additionally, current methods often use video features that include redundant information. In contrast, we propose MDSGen, a novel framework for open-domain sound synthesis based on a pure Transformer architecture. MDSGen incorporates a temporal-aware masking scheme and a redundant feature removal module, enabling it to achieve superior performance while being significantly more efficient. Further analysis highlights the effectiveness of our approach with compelling evidence of its advantages. Our contributions are as follows:

- We introduce a simple, lightweight, and efficient framework for open-domain sound generation using masked diffusion transformers, delivering high performance.
- Our approach implements Temporal-Awareness Masking (TAM), specifically designed for audio modality, in contrast to spatial-aware masking of the existing work, leading to more effective learning.
- We identify inefficiencies in the existing approach that fail to remove redundant video features. Our Reducer module learns to selectively resolve these redundancies, producing more refined features for improved audio generation.
- We validate our method on the benchmark datasets VGGSound and Flickr-SoundNet, surpassing state-of-the-art approaches across multiple metrics, with particularly significant improvements in alignment accuracy and efficiency, specifically in model parameters, memory consumption, and inference speed.

2 RELATED WORKS

2.1 OPEN-DOMAIN SOUND GENERATION

Auto-regressive Transformer-based Approach. Key works in this area include SpecVQGAN (Iashin & Rahtu, 2021), which uses a cross-modal Transformer to generate sounds from video tokens auto-regressively, and Im2Wav (Sheffer & Adi, 2023), which conditions audio token generation on CLIP features. However, these methods suffer from slow inference speeds due to their sequential generation process and limited vision-audio alignment, negatively impacting performance.

Diffusion-based Approach. To overcome these limitations, Diff-Foley (Luo et al., 2023) introduced a two-stage method that enhances semantic and temporal alignment via contrastive pre-training on aligned video-audio pairs, followed by latent diffusion for improved inference efficiency. Similarly, See and Hear (Xing et al., 2024) utilizes ImageBind (Girdhar et al., 2023) and AudioLDM (Liu et al., 2023) for various audio tasks, while FoleyCrafter (Zhang et al., 2024) combines a pre-trained text-to-audio model with a ControlNet-style module (Zhang et al., 2023) for high-quality, synchronized Foley generation. Although these diffusion approaches show promise, they often rely on large models with hundreds of millions of parameters and predominantly utilize U-Net architectures, leaving the potential of transformer-based architectures largely untapped.

Our proposed method leverages diffusion transformers (Peebles & Xie, 2023) and masking techniques for efficient learning. It also addresses the issue of redundant video features in Diff-Foley (Luo et al., 2023), which hinders further improvements in audio generation.

2.2 LATENT MASKED DIFFUSION TRANSFORMERS

The Denoising Diffusion Transformer (DiT) introduced by Peebles & Xie (2023) replaces the traditional U-Net with a fully transformer-based architecture for latent diffusion, demonstrating remarkable performance in large-scale image generation on ImageNet. Following this, Gao et al. (2023) proposed the Masked Diffusion Transformer (MDT), which enhances ImageNet generation through spatial context-aware masking. Inspired by MDT, Pham et al. (2024) developed X-MDPT, using cross-view masking to establish correspondence between pose and reference images for improved person image generation. Additionally, MDT-A2G (Mao et al., 2024) explored masked diffusion transformers for gesture generation, while QA-MDT (Li et al., 2024) adapted this technique for music generation.

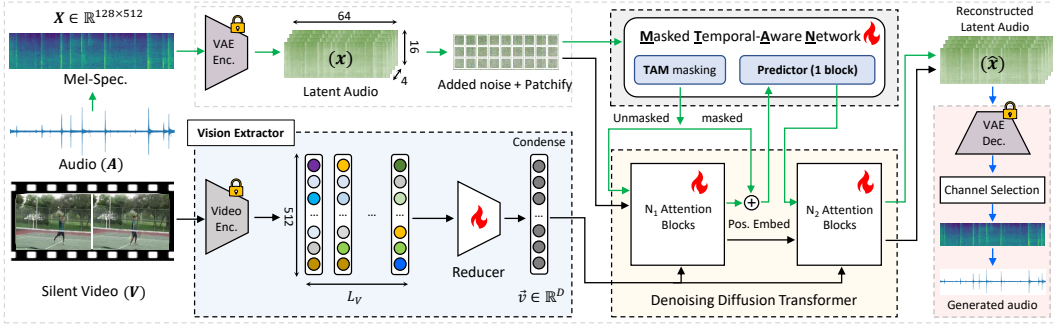


Figure 2: **Overview of the proposed highly-efficient MDSEn framework**, utilizing denoising masked diffusion transformers to efficiently learn video-conditional distributions for audio generation, replacing traditional Unet-based methods. The fire icon represents trainable modules, while the ‘locked’ icon indicates modules that remain frozen during training. Green arrows \rightarrow denote branches used only during training, blue arrows \rightarrow are for only inference, and black arrows \rightarrow are used in both training and inference.

In contrast to these works, we focus on lightweight masked diffusion models for video-guided audio generation, introducing temporal-aware masking for audio and a design that removes redundant video features to enhance generation effectiveness.

3 METHOD

We aim to develop a simple yet effective framework for vision-guided sound generation using transformers, addressing the limitations of existing approaches that rely on traditional U-Net architectures, which are less scalable and efficient. Our framework, illustrated in Fig. 2, consists of a novel **Vision Extractor** with a learnable **Reducer** that captures essential information from video input to generate a concise conditional output for the denoising diffusion process. This is followed by a **Denoising Diffusion Transformer** that maps Gaussian noise to sound distributions based on the extracted visual features. Additionally, we introduce a **Masked Temporal-Aware Network (MTANet)** that serves as a strong regularization mechanism for the transformer, enhancing overall performance. Finally, we incorporate **Channel Selection** for mel-spectrograms that further improves results.

3.1 DENOISING DIFFUSION TRANSFORMER

We adopt the DiT backbone introduced by Peebles & Xie (2023), which leverages transformers with self-attention during the denoising diffusion training process. Given an audio signal $\mathbf{A} \in \mathbb{R}^{L_A}$ of length L_A and a silent video $\mathbf{V} \in \mathbb{R}^{L_V \times 3 \times 224 \times 224}$ of length L_V , the audio is first transformed into a mel-spectrogram $\mathbf{X} \in \mathbb{R}^{128 \times 512}$, while the video is encoded into $\mathbf{v} \in \mathbb{R}^{L_V \times 512}$ and further reduced to $\tilde{\mathbf{v}} \in \mathbb{R}^{1 \times D}$. The mel-spectrogram is repeated across 3 channels, forming $\mathbf{X}' \in \mathbb{R}^{3 \times 128 \times 512}$, and passed through the VAE from Stable Diffusion (Rombach et al., 2022; Luo et al., 2023) to obtain a latent embedding $\mathbf{x} \in \mathbb{R}^{4 \times 16 \times 64}$. This latent representation is patched and tokenized into image tokens using a patch size of $p = 2$ (DiT’s default), resulting in $\mathbf{x}' \in \mathbb{R}^{256 \times D}$, where $L_{\mathbf{x}'} = 256$ and $D = 768$ for the B-size model. These tokens are then fed into the $N = N_1 + N_2$ self-attention layers of the Transformer to predict the noise ϵ added to the latent \mathbf{x} . Conditioned on the video encoding $\tilde{\mathbf{v}}$, the Transformer model ϕ learns the distribution $p_\phi(\mathbf{x}|\tilde{\mathbf{v}})$. During training, Gaussian noise $\epsilon \in \mathcal{N}(0, \mathbf{I})$ is added to the latent \mathbf{x} to generate \mathbf{x}_t at timestep $t \in [1, T]$. The overall training objective is:

$$\mathcal{L}_\Sigma = \mathbb{E}_{\mathbf{x}, \tilde{\mathbf{v}}, \epsilon} \|\epsilon - \epsilon_\phi(\mathbf{x}_t, \tilde{\mathbf{v}}, t)\|^2 + \lambda \mathbb{E}_{\mathbf{x}, \tilde{\mathbf{v}}, \epsilon} \|\epsilon - \epsilon_\phi(\mathcal{M}_\phi(\mathbf{x}_t), \tilde{\mathbf{v}}, t)\|^2. \quad (1)$$

Here, λ is the balance factor between the standard denoising diffusion loss (the first term in Eq. 1) and the masking loss (the second term), with $\lambda = 1.0$ for optimal performance. The masking function \mathcal{M}_ϕ , which includes the MTANet introduced later, applies temporal-aware masking. During inference, given a silent video, the model starts from Gaussian noise (no audio provided), and the predicted latent $\hat{\mathbf{x}} \in \mathbb{R}^{4 \times 16 \times 64}$ is iteratively denoised and decoded by the VAE decoder to recover the mel-spectrogram $\hat{\mathbf{X}}_{RGB} \in \mathbb{R}^{3 \times 128 \times 512}$. Channel selection refines this into $\hat{\mathbf{X}} \in \mathbb{R}^{128 \times 512}$, and the final waveform is reconstructed from the mel-spectrogram using the Griffin-Lim algorithm (Griffin & Lim, 1984), consistent with previous work (Luo et al., 2023) for fair comparison.

3.2 VISION EXTRACTOR

The second key component of our framework is the Vision Extractor with a learnable Reducer network that aligns video features with audio while condensing temporal information. We leverage the pre-trained CAVP model from (Luo et al., 2023), which was trained on Audioset using contrastive loss to extract video features aligned with audio. However, we identified that the CAVP features contain redundancies that could negatively impact generation quality. Diff-Foley (Luo et al., 2023) linearly maps original feature dimensions from $\mathbf{v} \in \mathbb{R}^{L_V \times 512}$ to $\mathbf{v} \in \mathbb{R}^{L_V \times 768}$ and retains this full dimensionality during the latent diffusion process via cross-attention, with L_V is the video feature length.

Our approach reduces the dimensionality to $\vec{v} \in \mathbb{R}^{1 \times 768}$, offering more concise and efficient information for denoising diffusion. Specifically, we project the encoded features $L_V \times 512$ through a multi-layer perceptron (MLP) into the transformer feature space ($L_V \times 768$ for the size B-model). These features are then passed through a reducer module, an 1×1 convolutional layer, which condenses the high-dimensional features into a lightweight form $\vec{v} \in \mathbb{R}^{1 \times 768}$. This compact representation is integrated into the denoising diffusion process through Adaptive LayerNorm (AdaLN) modulation. Unlike Diff-Foley, which retains all L_V video channels representing L_V video frames for cross-attention within the Stable Diffusion U-Net backbone, our method minimizes redundant features that could lead to overfitting. Our analysis shows that the L_V -**frame input features share over 90% similarity**, indicating considerable redundancies, which we further address in our ablation study.

Intuition. Our simple yet effective reducer design treats the temporal dimension of video ($L_V = 32$) as feature channels and performs a non-linear projection to a single channel, functioning similarly to channel attention by weighting important channels and summing them. This acts as a bottleneck that distills and distributes video temporal information across the 768 dimensions, aligning better with each audio token, which also has a 768-dimensional space. This approach, combined with the transformer network, significantly improves alignment accuracy up to approximately 99%.

3.3 AUDIO MASKED TEMPORAL-AWARE NETWORK

Thirdly, we introduce a novel technique that exploits the sound information’s natural characteristic: the temporal sense. The existing masking, **Spatial-Aware Mask** (SAM) proposed by MDT (Gao et al., 2023) is designed for image data to learn the spatial context within the image. But here, in the audio data (represented by mel-spectrogram with 2D data), the SAM masking method yields a sub-optimal solution because it cannot model the exact nature of temporal meaning in the audio data.

To overcome this limitation, we propose the **Temporal-Aware Mask** (TAM) strategy instead of SAM, which tries to mask the whole set of tokens along the temporal dimension. As shown in the ablation section, this novel masking helps significantly boost performance in all metrics compared to the existing method SAM specified for image data as shown in Fig. 3. Interestingly, despite this simple strategy, it can help the denoising transformer models learn to generate audio much better than random masks as used in existing MDT designed for image data.

During training, we mask with $\eta_m\%$ of temporal tokens, we feed only the visible tokens to the N_1 blocks of the transformer: $\mathbf{o}_1 = \text{Encoder}_{N_1}(\mathbf{x}' \odot (1 - \mathbf{m}))$ (\mathbf{m} is a mask matrix and \odot denotes element-wise multiplication) and in the MTANet we concatenate the resulting tokens with the learnable mask tokens \mathbf{M} and feed into a single block of predictor (referred to as side-interpolator in MDT) to achieve the full latent tokens before feeding into the final N_2 self-attention blocks of the transformer: $\mathbf{o}_2 = \text{Decoder}_{N_2}(\text{cat}(\mathbf{o}_1, \mathcal{M}_\phi(\mathbf{M} * \mathbf{x}' \odot (\mathbf{m}))))$. Here we find that different from the design for ImageNet with $N_2 = 2$ in the default MDT, we use $N_2 = 4$ which gives a better

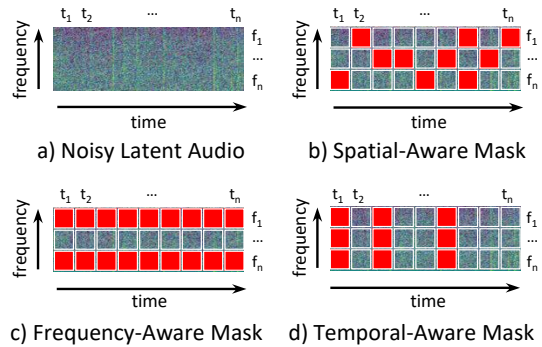


Figure 3: **Audio Masking Strategies.** Here, the red square is the learnable mask token.

performance for audio data. After training, the masked modeling branch is discarded, maintaining only its positional embedding for inference.

3.4 CLASSIFIER-FREE GUIDANCE

We adopt the dynamic Classifier-Free Guidance (CFG) method from previous works on masked diffusion transformer models (Gao et al., 2023) used in ImageNet. However, unlike image tasks, we find that in audio generation, the optimal CFG value is between 5 and 6, with a power scale of 0.01. Notably, Classifier-Guidance (CG) has been shown to significantly boost performance in Diff-Foley (Luo et al., 2023), where their method relies heavily on CG for optimal results. In contrast, our approach without CG surpasses Diff-Foley (CFG+CG) across multiple metrics. While incorporating CG improves our framework in terms of alignment accuracy and KL, it does not enhance other metrics. Hence, for simplicity, we omit CG in most of our experiments.

3.5 MEL-SPECTROGRAM CHANNEL SELECTION

We discovered that the audio extracted from the RGB output channels of the VAE decoder exhibits different qualities. Since the mel-spectrogram is 2D, we treat it as a single gray channel and duplicate it into three channels before feeding it into the VAE, which is pre-trained to reconstruct RGB images. At the decoding stage, the VAE outputs three channels: $\hat{\mathbf{X}}_{RGB} \in \mathbb{R}^{3 \times 128 \times 512}$, with $\hat{\mathbf{X}}_{RGB}[i, :, :] \in \mathbb{R}^{128 \times 512}$, $i \in \{0, 1, 2\}$ representing the R, G, and B channels. While Diff-Foley (Luo et al., 2023) used the first channel (R) as their final output, our empirical tests reveal that the second channel (G) consistently performs better. We further ablated channel selection and found that using the G channel yields superior results compared to the R channel used in prior work.

4 EXPERIMENTS

4.1 DATASET AND EVALUATION METRICS

(i) Dataset. We evaluate our method on the VGGSound dataset (Chen et al., 2020a), using the original train/test splits with 175k and 15k samples, respectively, and on the Flick-SoundNet dataset Aytar et al. (2016) with 5k test samples. **(ii) Metrics.** We first use the same metrics as prior work (Luo et al., 2023), including FID, IS, KL, and Alignment Accuracy, using their provided scripts for Align. Acc. and SpecVQGAN code for FID, IS, and KL. Second, we assess general vision-audio alignment in the Image2Audio task using CIoU and AUC metrics with scripts from (Mo & Morgado, 2022). For this, we generate pseudo videos by replicating a single input image for all frames. Third, we compare efficiency using parameter count, memory usage, and inference speed.

4.2 IMPLEMENTATION DETAILS

All models are trained and tested on a single A100 GPU (80GB) with a batch size of 64 and a learning rate of $5e-4$, using the Adan optimizer (Xie et al., 2024) for faster training. Unlike MDTv2 (Gao et al., 2023), we skip the macro-style of side interpolator design, as it was ineffective for our task, and instead use a simple self-attention block at decoder layer 4. Video-audio pairs are truncated to 8.2 seconds before encoding, following (Luo et al., 2023). Our model comes in three main variants: Tiny (5M), Small (33M), and Base (131M), with the Large (460M) variant showing overfitting. We primarily focus on the T, S, and B models.

4.3 MAIN RESULTS

A. VGGSound dataset. Compared to state-of-the-art approaches, our method significantly outperforms all competitors’ alignment accuracy while being far more efficient regarding parameters and inference speed (Tab. 1). Alignment accuracy, a metric introduced by (Luo et al., 2023), assesses synchronization and audio-visual relevance using a separate classifier trained to predict real audio-visual pairs. Remarkably, our Transformer-based model, MDSTGen-Tiny (5M), trained from scratch, achieves 97.9% accuracy, surpassing the second-best Diff-Foley (860M), which is $172\times$ larger and depends on a backbone of Stable Diffusion pre-trained on billion image-text pairs.

As shown in Tab. 1, Diff-Foley struggles without a pre-trained backbone, with a significant drop to FID 16.98 and IS 24.91. In contrast, our smallest model, `MDSGen-T` (5M), trained from scratch, achieves FID 14.18 and IS 37.51, emphasizing the overfitting issues of heavy U-Net-based models compared to our lightweight Transformers. Our larger model, `MDSGen-B` (131M), achieves state-of-the-art alignment accuracy ($\approx 99\%$) and an IS of 57.12 at 800k steps, though longer training leads to overfitting and declines in other metrics.

Table 1: **Benchmark on VGGSound test.** Generation quality comparison of different approaches. † gets from (Luo et al., 2023), ‡ denotes without pre-trained SDv1.4. * denotes results with pre-trained SDv1.4, we reproduce it using the public checkpoint.

| Method | FID↓ | IS↑ | KL↓ | Align. Acc.↑ | Time↓ (s) | #Params↓ | Cost↓ |
|-----------------------------------|--------------|--------------|-------------|--------------|-------------|-------------|-------|
| SpecVQGAN (Iashin & Rahtu, 2021)† | 9.70 | 30.80 | 7.03 | 49.19 | 5.47 | 308M | 61× |
| Im2Wav (Sheffer & Adi, 2023) † | 11.44 | 39.30 | 5.20 | 67.40 | 6.41 | 448M | 90× |
| Diff-Foley (Luo et al., 2023) †‡ | 16.98 | 24.91 | 6.05 | 92.61 | 0.38 | 860M | 172× |
| Diff-Foley (Luo et al., 2023) * | <u>10.55</u> | <u>56.67</u> | 6.49 | <u>93.92</u> | 0.36 | 860M | 172× |
| See and Hear (Xing et al., 2024) | 21.35 | 19.23 | 6.94 | 58.14 | 18.25 | 1099M | 220× |
| FoleyCrafter (Zhang et al., 2024) | 12.07 | 42.06 | <u>5.67</u> | 83.54 | 2.96 | 1252M | 250× |
| MDSGen-T (Ours) 500k | 14.18 | 37.51 | 6.25 | 97.91 | 0.01 | 5M | 1.0× |
| MDSGen-S (Ours) 500k | 12.92 | 44.38 | 6.29 | 98.32 | 0.02 | 33M | 6.6× |
| MDSGen-B (Ours) 500k | 11.19 | 52.77 | 6.27 | 98.55 | 0.05 | 131M | 26.2× |
| MDSGen-B (Ours) 800k | 12.29 | 57.12 | 6.43 | 91.62 | 0.05 | 131M | 26.2× |

B. Flickr_SoundNet dataset. We use the models trained on VGGSound to test on SoundNet dataset to evaluate its generalization. First, through quantitative metrics in the sound source localization task with Flickr-SoundNet (Aytar et al., 2016) test set. Second, qualitatively compare the generated audio across different methods. As shown in Tab. 2, our method outperforms other methods on the CIoU metric (82.01%) closer to the ground truth (83.94%), while the AUC remains comparable (around 55.5%). It shows that our generated audio provided better-aligned features with the visual information to localize the sound source. Diff-Foley performs worst, indicating that it is more overfitting. We provide their visualizations in the Appendix.

Table 2: **Benchmark on Flickr-SoundNet test.** Comparison of different approaches. ‘**Bold**’ and ‘underline’ denote the best and second-best, respectively.

| Method | CIoU↑ | AUC↑ |
|-----------------------------------|--------------|--------------|
| Diff-Foley (Luo et al., 2023) | 81.02 | 55.19 |
| See and Hear (Xing et al., 2024) | 81.20 | 55.45 |
| FoleyCrafter (Zhang et al., 2024) | 81.78 | 55.57 |
| MDSGen-B (Ours) 500k | 82.01 | <u>55.51</u> |
| Ground Truth | 83.94 | 63.60 |

5 ABLATION STUDY

We attribute the strong performance of our models to three key factors. First, the **Transformer backbone** enables more effective learning of the audio modality compared to existing Unet-based diffusion methods (Diff-Foley, See and Hear, FoleyCrafter). Second, our innovative **Reducer** module mitigates potential redundancies in the video input. Third, the **temporal masking model** acts as a robust regularizer, further enhancing the Transformer’s performance. A detailed analysis of these components is provided in the following sections.

5.1 ALIGNMENT ACCURACY: A CONFIDENCE SCORE PERSPECTIVE

We assess the enhancement of alignment accuracy in our method by analyzing confidence scores from the VGGSound test set, using the output of the sigmoid function from the trained classifier that predicts audio-video alignment. As illustrated in Fig. 4, FoleyCrafter (acc=83.54%) produces many low-confidence samples, indicating misalignment.

In contrast, Diff-Foley (93.9%) achieves a higher proportion of high-confidence scores. Remarkably, our method reaches an accuracy of 98.6%, significantly increasing the number of high-confidence samples and demonstrating superior audio-video alignment compared to other approaches.

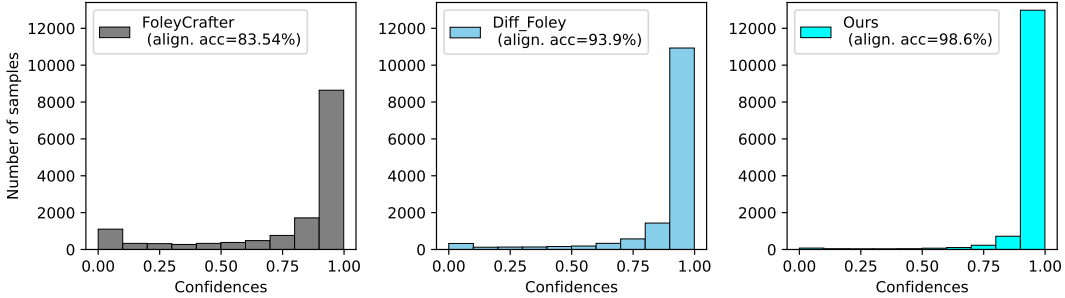


Figure 4: **Confidence Scores.** Compared to FoleyCrafter (left) and Diff-Foley (middle), our method (right) produces many more audio samples with higher confidence that align with their corresponding videos on the VGGSound test set ($\sim 15k$ samples).

5.2 FEATURE DIMENSIONALITY REDUCTION AND REDUNDANT FEATURES IN CAVP

Unlike Diff-Foley, which uses a U-Net-based Stable Diffusion model and incorporates all 32 video frame features for cross-attention, we found that reducing video features from 32 channels to a single channel significantly improves audio generation performance across all metrics (Tab. 3). Diff-Foley’s CAVP encodes video features at 32×512 , aligning with the audio’s 32-channel representation (also 32×512) for latent-level alignment via contrastive learning. However, in the second stage, a mismatch arises as the VAE reduces audio dimensions to $4 \times 16 \times 64$ while video expands to 32×768 , leading to redundancy and inefficiencies. Reducing video dimensionality to 1×768 representation acts as a bottleneck, simplifying learning and enhancing alignment, as supported by our results.

Analysis of the CAVP features in Diff-Foley shows significant redundancy, with cosine similarity averaging **0.9087** for real videos and **0.9233** for identical frames (Tab. 4). These high similarity scores suggest that the feature vectors from multiple frames largely overlap, limiting the model’s ability to learn distinctive characteristics essential for effective audio synthesis. This issue worsens when Diff-Foley expands features to a 32×768 dimension, diluting key traits for latent diffusion modeling. In contrast, our approach employs a Reducer module to consolidate the 32 video frame features into a 768-dimensional representation, effectively reducing redundancy and enhancing focus on salient features, which improves alignment accuracy and overall performance in audio generation tasks.

Table 3: **Dimension Reduction.** Compare the original CAVP and Ours’s features.

| Video Feat. | Cond. Dim. | FID | IS | KL | Align. Acc. |
|----------------|-----------------|--------------|--------------|-------------|--------------|
| Original CAVP | 32×768 | 13.55 | 50.12 | 6.38 | 96.18 |
| Reduced (Ours) | 1×768 | 11.19 | 52.77 | 6.27 | 98.55 |

Table 4: **Redundant Features.** Cosine similarity between the frame’s features.

| Input | Similarity (CAVP) |
|-------|-------------------|
| Video | 0.9087 |
| Image | 0.9233 |

5.3 CHANNEL SELECTION FROM RGB FOR MEL-SPECTROGRAM

Each R, G, and B channel exhibits distinct characteristics, as noted in previous research (Xu et al., 2017). In the VAE encoder, we replicate the gray mel-spectrogram across three identical channels, but the VAE decoder does not enforce channel consistency. Our analysis shows that the RGB output $\hat{\mathbf{X}}_{RGB}$ retains unique statistical differences across channels (see Fig. 5), influencing their contributions to the final mel-spectrogram and waveform. In contrast to Diff-Foley, which uses only the R channel ($\hat{\mathbf{X}}_{RGB}[0, :, :]$) for the final mel-spectrogram, we find the G channel ($\hat{\mathbf{X}}_{RGB}[1, :, :]$) to be optimal (see Tab. 5). Fig. 5 shows that the histograms of the three VAE output channels display significant differences, with the G and B channels aligning closely with the ground truth distribution.

Table 5: **Channel selection for mel-spectrogram.** Gray indicates the default.

| Channel | FID↓ | IS↑ | KL↓ | Align. Acc.↑ (%) |
|--|--------------|--------------|-------------|------------------|
| $R (i = 0)$ | 11.40 | 51.54 | 6.29 | 98.51 |
| $G (i = 1)$ | 11.19 | 52.77 | 6.27 | 98.55 |
| $B (i = 2)$ | 11.23 | 52.32 | 6.27 | 98.56 |
| $\frac{1}{3} \sum_{r \in \{R, G, B\}} r$ | 11.29 | 52.27 | 6.28 | 98.54 |

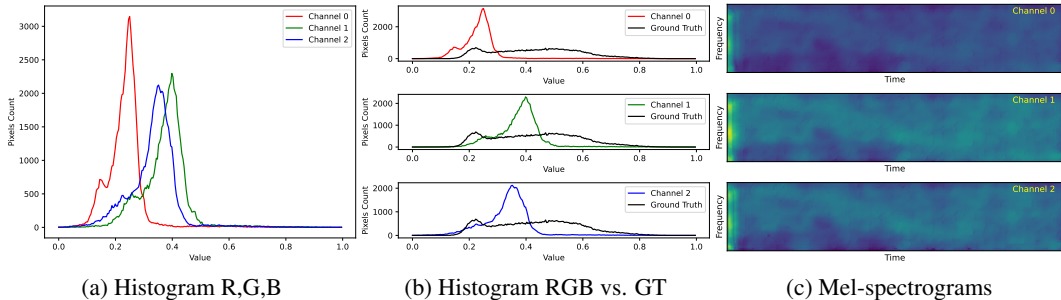


Figure 5: Histogram and mel-spectrogram comparison of three channels of VAE output.

Notably, while the resulting mel-spectrograms (right figures) seem visually indistinguishable, the histograms highlight their differences. This emphasizes the importance of considering each channel’s statistics in generating the final mel-spectrogram \hat{X} , with further comparisons available in the Appendix.

5.4 MASKING DIFFUSION STRATEGIES

We explore various audio-masking methods in diffusion transformers (Fig. 3) and compare them to traditional image-based techniques like SAM used with ImageNet (Gao et al., 2023). Our findings reveal that audio data behaves differently from images (SAM), with incorporating temporal awareness (TAM) into the masking task significantly boosting performance across all metrics (Tab. 6), including a 4-point IS score increase from 48.66 to 52.77. Using a diffusion transformer without masking (DiT) leads to suboptimal results across all metrics, highlighting the critical role of masking in model learning.

Table 6: **Masking Strategy for Audio Generation.** Comparison of different ways to train diffusion transformer-based models. Masking on temporal audio gives the best performance.

| Masking Method | Mask | Temporal | FID↓ | IS↑ | KL↓ | Align. Acc.↑ (%) |
|--------------------------------|------|----------|--------------|--------------|-------------|------------------|
| DiT (Peebles & Xie, 2023) | × | × | 14.55 | 46.11 | 6.51 | 97.12 |
| Random, SAM (Gao et al., 2023) | ✓ | × | 12.44 | 48.66 | 6.30 | 98.15 |
| Frequency, FAM | ✓ | × | 12.79 | 46.33 | 6.41 | 97.58 |
| Temporal, TAM (Ours) | ✓ | ✓ | 11.19 | 52.77 | 6.27 | 98.55 |

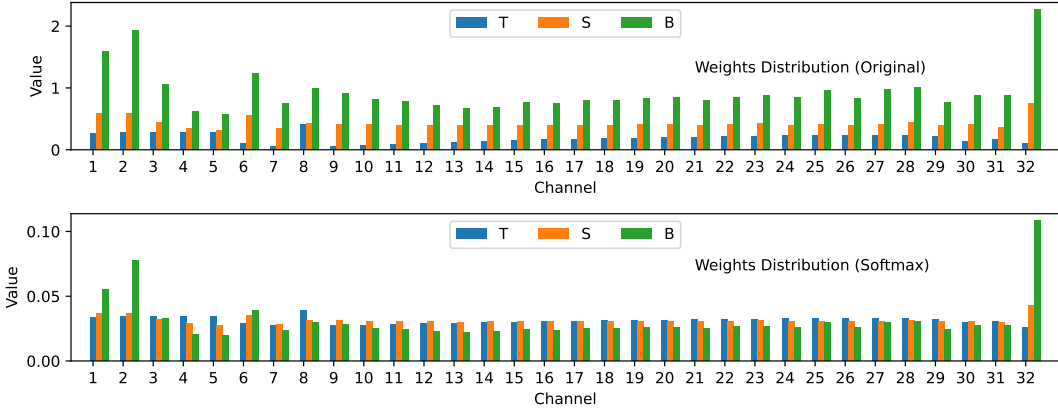
5.5 LEARNED WEIGHTS OF REDUCER

We analyzed how our models allocate attention across video frames by visualizing their learned magnitude weights (Fig. 6). The upper figure shows that our model applies varying attention levels, with larger models exhibiting higher weights and more distinct differences. After softmax normalization (bottom figure), consistent trends are observed for various channels, though not all, with model B focusing more on channels 1, 2, and 32. These findings demonstrate that the Reducer effectively captures key features, selectively updating weights to prioritize relevant ones for audio generation.

5.6 SCALABILITY

We evaluate the scalability of MDSTGen, the first to explore ViT-based masked diffusion models for vision-guided audio generation. Results in Tab. 7 show that increasing the model size from T to B improves all metrics. However, further scaling to the L model leads to a performance drop, indicating potential overfitting at larger sizes.

5.7 SAMPLING TOOLS

Figure 6: **Learned Weights of Reducer.** Comparison of our three models.Table 7: **Scalability.** We ablate four variants Tiny (T), Small (S), Base (B), and Large (L).

| Model Config. | FID↓ | IS↑ | KL↓ | Align. Acc.↑ | #Params | #Layers | Dim. | #Heads |
|---------------|--------------|--------------|-------------|--------------|---------|---------|------|--------|
| MDSGen-T | 13.93 | 39.24 | 6.17 | 97.9 | 5M | 12 | 192 | 3 |
| MDSGen-S | 12.92 | 44.38 | 6.29 | 98.3 | 33M | 12 | 384 | 6 |
| MDSGen-B | 11.19 | 52.77 | 6.27 | 98.6 | 131M | 12 | 768 | 12 |
| MDSGen-L | 12.68 | 49.53 | 6.56 | 97.9 | 461M | 24 | 1024 | 16 |

Sampling Method. We employ DPM-Solver (Lu et al., 2022) with 25 steps for sampling during inference. We find that increasing from 25 to 50 steps with dynamic classifier-free guidance (Gao et al., 2023) can slightly improve the performance. We used CFG = 5 and power scaling $\alpha = 0.01$ for the optimal setting. **Classifier-Guidance (CG).** We found that combining CFG and CG slightly improves alignment accuracy and KL, consistent with (Luo et al., 2023), but has no impact on other metrics (see Tab. 8), which differs from their findings. A thorough investigation of network architecture and additional datasets is needed to assess the complementary effects of CFG and CG fully, but this is beyond the scope of our work.

Table 8: **CFG and CG.** We examine the effect of classifier-free guidance and classifier guidance. Results are shown with model MDSGen-B. Gray indicates the default.

| Setup | FID↓ | IS↑ | KL↓ | Align. Acc.↑ |
|-------------|--------------|--------------|-------------|--------------|
| No Guidance | 16.50 | 23.54 | 6.85 | 84.1 |
| CFG | 11.19 | 52.77 | 6.27 | 98.6 |
| CFG + CG | 11.25 | 51.48 | 6.24 | 98.8 |

5.8 COMPARE THE EFFICIENCY

We evaluated inference time, parameter count, and memory usage on a single A100 GPU (80GB) with batch size 1. Tab. 9 shows our method is significantly faster, uses fewer parameters, and consumes less memory than existing methods. Specifically, Diff-Foley (860M) achieves 93.9% alignment accuracy with a 0.36s inference time, while our MDSGen-T (5M) reaches

Table 9: **Efficiency Comparison.** Our approach is simple and highly efficient across all metrics, with superior alignment accuracy compared to existing methods.

| Method | Time↓ | Mem. Use↓ | #Params↓ | Align. Acc.↑ |
|-----------------------------------|--------------|--------------|-------------|--------------|
| Im2Wav (Sheffer & Adi, 2023) | 6.41s | 1684M | 448M | 67.4 |
| See and Hear (Xing et al., 2024) | 18.25s | 14466M | 1280M | 58.1 |
| FoleyCrafter (Zhang et al., 2024) | 2.96s | 12908M | 1252M | 83.5 |
| Diff-Foley (Luo et al., 2023) | 0.36s | 5228M | 860M | 93.9 |
| MDSGen-T (Ours) | 0.01s | 1406M | 5M | 97.9 |
| MDSGen-S (Ours) | 0.02s | 1508M | 33M | 98.3 |
| MDSGen-B (Ours) | 0.05s | 2132M | 131M | 98.6 |

97.9% in just 0.01s, 36× faster and 371% more memory efficient. Our larger model MDSGen-B (131M) improves accuracy to 98.6%, still 7.2× faster and 245% more memory efficient than Diff-Foley. Compared to FoleyCrafter and See and Hear, MDSGen-T is 296× and 1825× faster, respectively, while being 10× more memory efficient. We provide additional details on training efficiency in the Appendix, further emphasizing the remarkable efficiency of our approach.

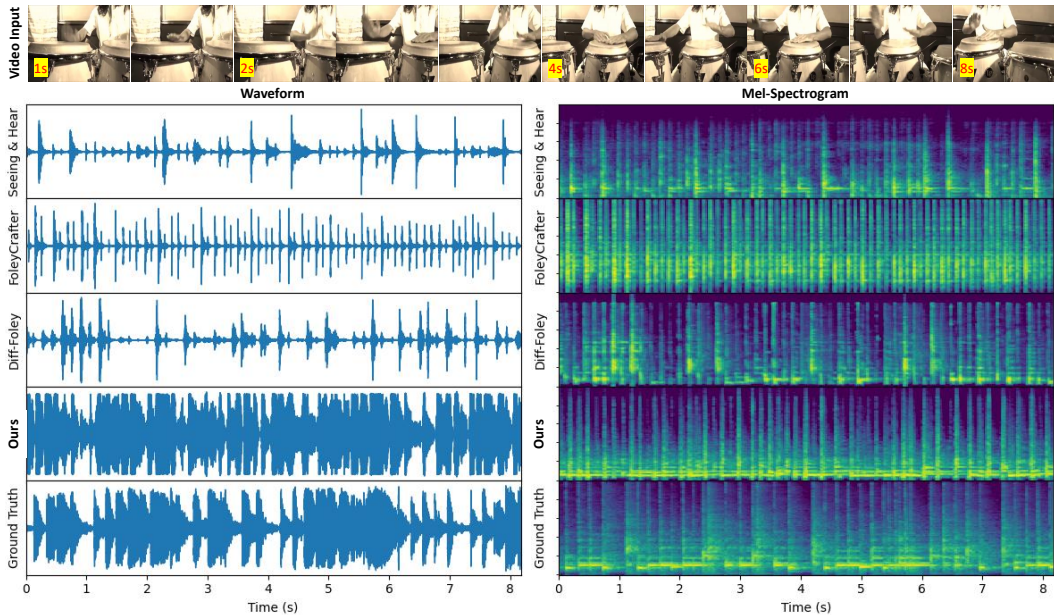


Figure 7: **Waveform and Mel-Spectrogram Comparison.** Sample is taken from the test set of the VGGSound dataset. Our model generates sound more closely aligned with the ground truth than existing methods. **The video of a woman playing drum by hand**, demo file “0NIE-eDk92M_000029.wav” is available in the supplementary material.

5.9 VISUALIZATIONS

We visualize different approaches using test video samples from the VGGSound dataset. As shown in Fig. 7, our method generates mel-spectrograms that closely match the ground truth (right figure), with even clearer distinctions observable in the waveform (left figure). Additional demo samples, along with WAV files for convenient listening and their visualizations, are included in the Appendix and supplementary material.

6 CONCLUSIONS

This work presents a novel, scalable, and highly efficient framework for video-guided audio generation. Leveraging Diffusion Transformers, we introduced an innovative masking strategy that enhances the model’s ability to capture temporal dynamics in audio, leading to significant performance gains. To address redundant video features, we introduced a Reducer module to eliminate unnecessary information. Extensive experiments and detailed analyses demonstrate that our model achieves fast training and inference times, uses minimal parameters, and delivers superior performance across multiple metrics, setting a new benchmark in the field.

7 LIMITATIONS AND FUTURE WORKS

Our method offers fast inference, efficient parameter, and memory usage, and achieves top performance in alignment accuracy and IS score. However, it does have some limitations. First, like other diffusion models, it requires multiple sampling steps during generation. Second, while the VGGSound dataset is suitable for this study, it is not a large-scale dataset, which may not fully exploit the potential of our approach. Third, the current design handles a fixed video length of 8.2 seconds. We hope to incorporate recent advancements in single-step diffusion techniques into our framework in the future. Additionally, while video collection from online sources is increasingly feasible, it can still be time-consuming and storage-intensive, posing challenges for individual researchers. We leave further exploration in this area, along with addressing the fixed-length constraint, for future work.

REFERENCES

- Vanessa Theme Ament. *The Foley grail: The art of performing sound for film, games, and animation*. Routledge, 2014. 1
- Yusuf Aytar, Carl Vondrick, and Antonio Torralba. Soundnet: Learning sound representations from unlabeled video. *Advances in neural information processing systems*, 29, 2016. 5, 6
- Andreas Blattmann, Robin Rombach, Huan Ling, Tim Dockhorn, Seung Wook Kim, Sanja Fidler, and Karsten Kreis. Align your latents: High-resolution video synthesis with latent diffusion models. In *Proceedings of the IEEE/CVF Conference on Computer Vision and Pattern Recognition*, pp. 22563–22575, 2023. 1
- Honglie Chen, Weidi Xie, Andrea Vedaldi, and Andrew Zisserman. Vggsound: A large-scale audio-visual dataset. In *ICASSP 2020-2020 IEEE International Conference on Acoustics, Speech and Signal Processing (ICASSP)*, pp. 721–725. IEEE, 2020a. 5
- Peihao Chen, Yang Zhang, Mingkui Tan, Hongdong Xiao, Deng Huang, and Chuang Gan. Generating visually aligned sound from videos. *IEEE Transactions on Image Processing*, 29:8292–8302, 2020b. 1
- Shanghai Gao, Pan Zhou, Ming-Ming Cheng, and Shuicheng Yan. Masked diffusion transformer is a strong image synthesizer. *arXiv preprint arXiv:2303.14389*, 2023. 2, 4, 5, 8, 9
- Rohit Girdhar, Alaeldin El-Nouby, Zhuang Liu, Mannat Singh, Kalyan Vasudev Alwala, Armand Joulin, and Ishan Misra. Imagebind: One embedding space to bind them all. In *Proceedings of the IEEE/CVF Conference on Computer Vision and Pattern Recognition*, pp. 15180–15190, 2023. 2
- Daniel Griffin and Jae Lim. Signal estimation from modified short-time fourier transform. *IEEE Transactions on acoustics, speech, and signal processing*, 32(2):236–243, 1984. 3
- Kaiming He, Xinlei Chen, Saining Xie, Yanghao Li, Piotr Dollár, and Ross Girshick. Masked autoencoders are scalable vision learners. In *Proceedings of the IEEE/CVF conference on computer vision and pattern recognition*, pp. 16000–16009, 2022. 16
- Hanzhuo Huang, Yufan Feng, Cheng Shi, Lan Xu, Jingyi Yu, and Sibe Yang. Free-bloom: Zero-shot text-to-video generator with llm director and ldm animator. *Advances in Neural Information Processing Systems*, 36, 2024. 1
- Vladimir Iashin and Esa Rahtu. Taming visually guided sound generation. In *British Machine Vision Conference*, 2021. 1, 2, 6
- Young Hoon Jung, Seong Kwang Hong, Hee Seung Wang, Jae Hyun Han, Trung Xuan Pham, Hyunsin Park, Junyeong Kim, Sunghun Kang, Chang D Yoo, and Keon Jae Lee. Flexible piezoelectric acoustic sensors and machine learning for speech processing. *Advanced Materials*, 32(35):1904020, 2020. 16
- Young Hoon Jung, Trung Xuan Pham, Dias Issa, Hee Seung Wang, Jae Hee Lee, Mingi Chung, Bo-Yeon Lee, Gwangsu Kim, Chang D Yoo, and Keon Jae Lee. Deep learning-based noise robust flexible piezoelectric acoustic sensors for speech processing. *Nano Energy*, 101:107610, 2022. 16
- Levon Khachatryan, Andranik Movsisyan, Vahram Tadevosyan, Roberto Henschel, Zhangyang Wang, Shant Navasardyan, and Humphrey Shi. Text2video-zero: Text-to-image diffusion models are zero-shot video generators. In *Proceedings of the IEEE/CVF International Conference on Computer Vision*, pp. 15954–15964, 2023. 1
- Junyeong Kim, Minuk Ma, Trung Pham, Kyungsu Kim, and Chang D Yoo. Modality shifting attention network for multi-modal video question answering. In *Proceedings of the IEEE/CVF conference on computer vision and pattern recognition*, pp. 10106–10115, 2020. 16
- Donghoon Lee, Hyunsin Park, Trung Pham, and Chang D Yoo. Learning augmentation network via influence functions. In *Proceedings of the IEEE/CVF Conference on Computer Vision and Pattern Recognition*, pp. 10961–10970, 2020. 16

- Chang Li, Ruoyu Wang, Lijuan Liu, Jun Du, Yixuan Sun, Zilu Guo, Zhenrong Zhang, and Yuan Jiang. Quality-aware masked diffusion transformer for enhanced music generation. *arXiv preprint arXiv:2405.15863*, 2024. [2](#)
- Haohe Liu, Zehua Chen, Yi Yuan, Xinhao Mei, Xubo Liu, Danilo Mandic, Wenwu Wang, and Mark D Plumbley. Audioldm: Text-to-audio generation with latent diffusion models. In *International Conference on Machine Learning*, pp. 21450–21474. PMLR, 2023. [2](#)
- Cheng Lu, Yuhao Zhou, Fan Bao, Jianfei Chen, Chongxuan Li, and Jun Zhu. Dpm-solver++: Fast solver for guided sampling of diffusion probabilistic models. *arXiv preprint arXiv:2211.01095*, 2022. [9](#)
- Simian Luo, Chuanhao Yan, Chenxu Hu, and Hang Zhao. Diff-foley: Synchronized video-to-audio synthesis with latent diffusion models. *Advances in Neural Information Processing Systems*, 36, 2023. [1](#), [2](#), [3](#), [4](#), [5](#), [6](#), [9](#), [14](#)
- Xiaofeng Mao, Zhengkai Jiang, Qilin Wang, Chencan Fu, Jiangning Zhang, Jiafu Wu, Yabiao Wang, Chengjie Wang, Wei Li, and Mingmin Chi. Mdt-a2g: Exploring masked diffusion transformers for co-speech gesture generation. *arXiv preprint arXiv:2408.03312*, 2024. [2](#)
- Shentong Mo and Pedro Morgado. Localizing visual sounds the easy way. In *European Conference on Computer Vision*, pp. 218–234. Springer, 2022. [5](#), [14](#)
- Axi Niu, Kang Zhang, Trung X Pham, Jinqiu Sun, Yu Zhu, In So Kweon, and Yanning Zhang. Cdpmsr: Conditional diffusion probabilistic models for single image super-resolution. In *2023 IEEE International Conference on Image Processing (ICIP)*, pp. 615–619. IEEE, 2023. [16](#)
- Axi Niu, Trung X Pham, Kang Zhang, Jinqiu Sun, Yu Zhu, Qingsen Yan, In So Kweon, and Yanning Zhang. Acdmsr: Accelerated conditional diffusion models for single image super-resolution. *IEEE Transactions on Broadcasting*, 2024a. [16](#)
- Axi Niu, Kang Zhang, Trung X Pham, Pei Wang, Jinqiu Sun, In So Kweon, and Yanning Zhang. Learning from multi-perception features for real-word image super-resolution. *IEEE Transactions on Circuits and Systems for Video Technology*, 2024b. [16](#)
- Yichen Ouyang, Hao Zhao, Gaoang Wang, et al. Flexifilm: Long video generation with flexible conditions. *arXiv preprint arXiv:2404.18620*, 2024. [1](#)
- William Peebles and Saining Xie. Scalable diffusion models with transformers. In *Proceedings of the IEEE/CVF International Conference on Computer Vision*, pp. 4195–4205, 2023. [2](#), [3](#), [8](#), [14](#)
- Trung Pham, Chaoning Zhang, Axi Niu, Kang Zhang, and Chang D Yoo. On the pros and cons of momentum encoder in self-supervised visual representation learning. *arXiv preprint arXiv:2208.05744*, 2022a. [16](#)
- Trung X Pham, Rusty John Lloyd Mina, Dias Issa, and Chang D Yoo. Self-supervised learning with local attention-aware feature. *arXiv preprint arXiv:2108.00475*, 2021. [16](#)
- Trung X. Pham, Kang Zhang, and Chang D. Yoo. Cross-view masked diffusion transformers for person image synthesis. In *Forty-first International Conference on Machine Learning*, 2024. [2](#)
- Trung Xuan Pham, Rusty John Lloyd Mina, Thanh Nguyen, Sultan Rizky Madjid, Jinwoong Choi, and Chang Dong Yoo. Lad: A hybrid deep learning system for benign paroxysmal positional vertigo disorders diagnostic. *IEEE Access*, 2022b. [16](#)
- Trung Xuan Pham, Axi Niu, Kang Zhang, Tee Joshua Tian Jin, Ji Woo Hong, and Chang D Yoo. Self-supervised visual representation learning via residual momentum. *IEEE Access*, 2023. [16](#)
- Robin Rombach, Andreas Blattmann, Dominik Lorenz, Patrick Esser, and Björn Ommer. High-resolution image synthesis with latent diffusion models. In *Proceedings of the IEEE/CVF conference on computer vision and pattern recognition*, pp. 10684–10695, 2022. [3](#), [14](#), [15](#)
- Roy Sheffer and Yossi Adi. I hear your true colors: Image guided audio generation. In *ICASSP 2023-2023 IEEE International Conference on Acoustics, Speech and Signal Processing (ICASSP)*, pp. 1–5. IEEE, 2023. [2](#), [6](#), [9](#)

- Pham Xuan Trung and Chang D Yoo. Short convolutional neural network and mfccs for accurate speaker recognition systems. *International Technical Conference on Circuits/Systems, Computers and Communications (ITC-CSCC)*, 2019. [16](#)
- Thang Vu, Hyunjun Jang, Trung X Pham, and Chang Yoo. Cascade rpn: Delving into high-quality region proposal network with adaptive convolution. *Advances in neural information processing systems*, 32, 2019. [16](#)
- Xingyu Xie, Pan Zhou, Huan Li, Zhouchen Lin, and Shuicheng Yan. Adan: Adaptive nesterov momentum algorithm for faster optimizing deep models. *IEEE Transactions on Pattern Analysis and Machine Intelligence*, 2024. [5](#)
- Yazhou Xing, Yingqing He, Zeyue Tian, Xintao Wang, and Qifeng Chen. Seeing and hearing: Open-domain visual-audio generation with diffusion latent aligners. In *Proceedings of the IEEE/CVF Conference on Computer Vision and Pattern Recognition*, pp. 7151–7161, 2024. [1](#), [2](#), [6](#), [9](#)
- Jian Xu, Zhiguo Chang, Jiulun Fan, Xiaoqiang Zhao, Xiaomin Wu, Yanzi Wang, and Xiaodan Zhang. Super-resolution via adaptive combination of color channels. *Multimedia Tools and Applications*, 76:1553–1584, 2017. [7](#)
- Lvmin Zhang, Anyi Rao, and Maneesh Agrawala. Adding conditional control to text-to-image diffusion models, 2023. [2](#)
- Yiming Zhang, Yicheng Gu, Yanhong Zeng, Zhening Xing, Yuancheng Wang, Zhizheng Wu, and Kai Chen. Foleyrafter: Bring silent videos to life with lifelike and synchronized sounds. *arXiv preprint arXiv:2407.01494*, 2024. [1](#), [2](#), [6](#), [9](#)

A APPENDIX

A.1 TRAINING COST

We leveraged the pre-trained VAE encoder and decoder from Stable Diffusion (Rombach et al., 2022), keeping them frozen during training and inference, similar to Diff-Foley. Our training utilized a single A100 GPU (80GB) with a batch size 64. The B-model (131M) is projected to take 4 days for 500k iterations, while the S-model (33M) and T-model (5M) are expected to finish in 3.3 and 2.8 days, respectively.

In comparison, the second-best method, the Diff-Foley approach (860M model) required 8 A100 GPUs with a batch size of 1760, completing 24.4k steps in 60 hours (2.5 days) (Luo et al., 2023). If scaled to a single A100 GPU, Diff-Foley would need at least 20 days more than a fifth of the time of our method, demonstrating the superior efficiency and significantly lower training costs of our approach (see Tab. 10).

Table 10: **Training Comparison.** Estimated for a single A100 GPU training. Our approach is simple and highly efficient compared to the second-best method Diff-Foley which used the heavy backbone of Stable Diffusion with 860M.

| Method | #Training cost↓ | Align. Acc.↑ |
|--------------------------------------|-----------------|--------------|
| Diff-Foley (860M) (Luo et al., 2023) | 20 days | 93.9 |
| MDSGen-T, 5M (Ours) | 2.8 days | 97.9 |
| MDSGen-S, 33M (Ours) | 3.3 days | 98.3 |
| MDSGen-B, 131M (Ours) | 4.1 days | 98.6 |

A.2 MORE SETUPS

We apply classifier-free guidance during training by randomly setting \vec{v} to zero with a 10% probability. Models are trained for 500k steps to ensure optimal convergence. The exponential moving average of the model weight is set to 0.9999, otherwise, settings are the same as default DiT (Peebles & Xie, 2023). No video augmentation is used; instead, we pre-extract and save lightweight video features for faster training. We also use a ratio of $\eta_m = 0.3$ by default for masking the temporal set of tokens. Our code will be made publicly available.

For experiments involving classifier guidance, we utilized the classifier trained by Diff-Foley, adjusting the optimal CG value to 2.0, compared to 50 in their framework. To evaluate alignment accuracy, we used their trained classifier to assess our generated audio. We also reproduced Diff-Foley’s performance using their published checkpoint, with results closely matching their reported metrics.

The slight variation may stem from differences in the VGGSound test set, as we download videos from several months to one year after their experiments, during which some original YouTube links may have been removed, causing potential mismatches.

A.3 COMPARING MORE VISUALIZATIONS

Gradcam Visualization of localization on VGGSound and Flickr-SoundNet datasets.

We used the generated audio to perform the sound source localization on each frame of the video and image using the pre-trained model of EZ-VSL (Mo & Morgado, 2022). As shown in Fig. 8 and Fig. 9, our method provides a more accurate attention map.

More generated audio comparison with state-of-the-art approaches on VGGSound test set.

We also provide more samples in the supplementary and their visualizations in Fig. 10, Fig. 11, Fig. 13, Fig. 14, and Fig. 12. As shown in these figures and listened to by authors, our generated audio is much more reasonable than others. We refer readers to examine the quality of generated audio in the submitted supplementary materials.

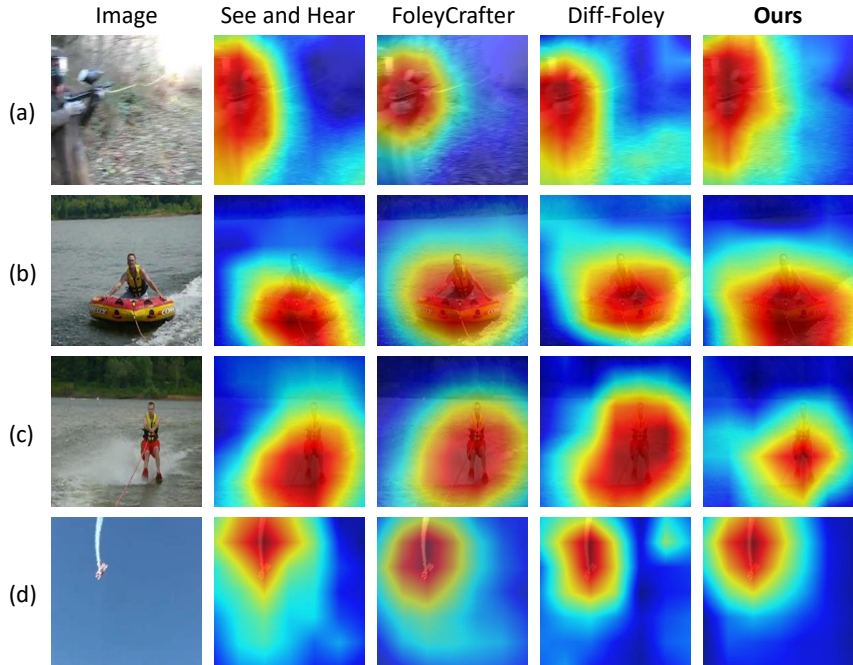


Figure 8: **Attention map Flickr-SoundNet dataset.** Our best model (MDSGen-B) generated the sound that contain information that help localize the sound source more accurately compared to existing approaches.

A.4 RGB CHANNEL SELECTION FOR MEL-SPECTROGRAM

We provide additional statistics of various generated audio samples, highlighting the differing characteristics of the VAE decoder outputs in Fig. 15 and Fig. 16. As shown, although the VAE encoder input consists of three identical channels, the generated outputs display distinct distributions across each channel (left figures), even though these differences are imperceptible to the human eye (right figures). This behavior stems from the fact that the VAE encoder and decoder in Stable Diffusion (Rombach et al., 2022) are trained exclusively for image data, where the R, G, and B channels inherently carry different information.

Because this model is applied directly to audio data without adaptation, there is no constraint ensuring the R, G, and B channels remain identical in the generated audio. Developing a method to adaptively select or combine these channels when constructing the final Mel-spectrogram could be a promising avenue for improving the quality of the generated audio.

A.5 MASK RATIO ABLATION

Tab. 11 shows that while a higher masking ratio maintains high alignment accuracy, it leads to declines in other metrics. This occurs because the transformer models prioritize audio token reconstruction over the primary generation task, resulting in worsened FID, IS, and KL scores.

Table 11: **Masking Strategy for Audio Synthesis.** Comparison of different ways to train diffusion transformer-based models. Masking on temporal audio gives the best performance.

| Masking Ratio | FID↓ | IS↑ | KL↓ | Align. Acc.↑ (%) |
|---------------|--------------|--------------|-------------|------------------|
| 70% | 12.85 | 44.42 | 6.38 | 97.86 |
| 50% | 12.39 | 46.77 | 6.38 | 98.43 |
| 30% | 11.19 | 52.77 | 6.27 | 98.55 |

A.6 MORE DIRECTIONS

Our approach can inspire applications of masked diffusion models across various domains such as object detection (Vu et al., 2019), video question answering (Kim et al., 2020), image super-resolution (Niu et al., 2024a;b), and speech processing. These models can also be combined with self-supervised learning techniques (He et al., 2022; Pham et al., 2021; 2022b; 2023; 2022a) to enhance representation learning for diverse generative tasks. With the potential of diffusion transformers for conditional learning, we anticipate further exploration of their capabilities in speech processing (Jung et al., 2022; 2020; Trung & Yoo, 2019), data augmentation (Lee et al., 2020), VQA (Kim et al., 2020), visual detection (Vu et al., 2019), and super-resolution (Niu et al., 2023; 2024a;b).

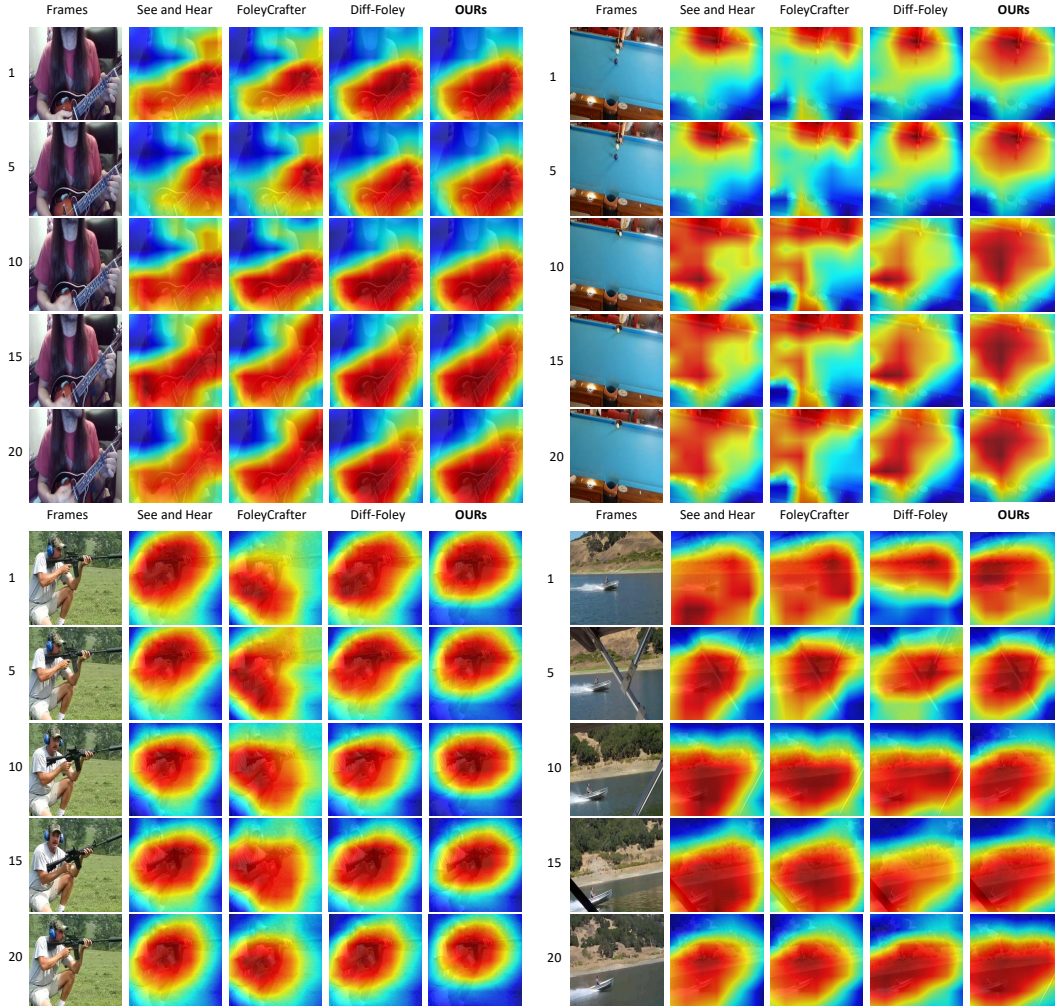


Figure 9: **Attention map VGGSound dataset.** Our best model (MDSGen-B) generated the sound that contain information that help localize the sound source more accurately compared to existing approaches.

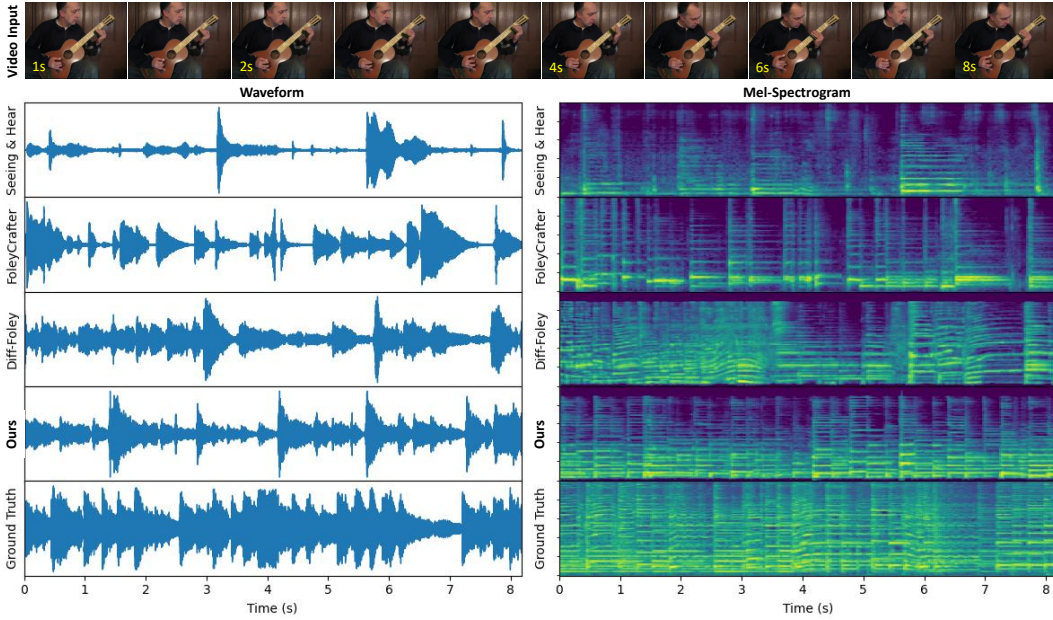


Figure 10: **The video of a man playing guitar solo.** Our best model (MDSGen-B) generated a sound that is closer to GT compared to existing approaches. We refer the reader to the listen file provided in the supplementary for comparison. File “-IPXTBXa0tE_000030.wav”.

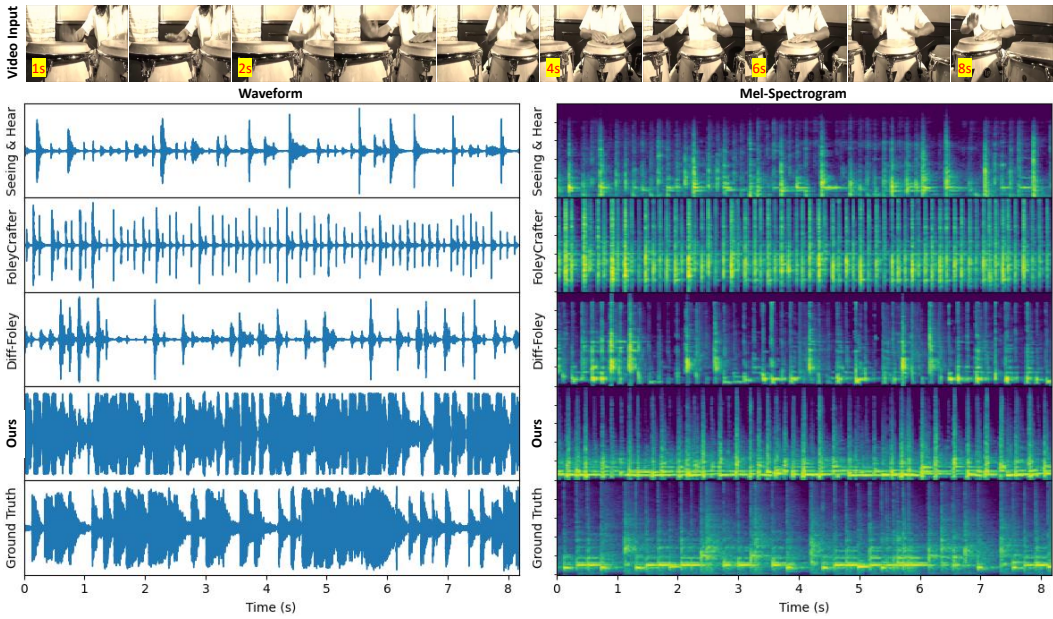


Figure 11: **The video of a woman playing drum by hand.** Our best model (MDSGen-B) generated a sound that is closer to GT compared to existing approaches. We refer the reader to the listen file provided in the supplementary for comparison. File “0NIE-eDk92M_000029.wav”.

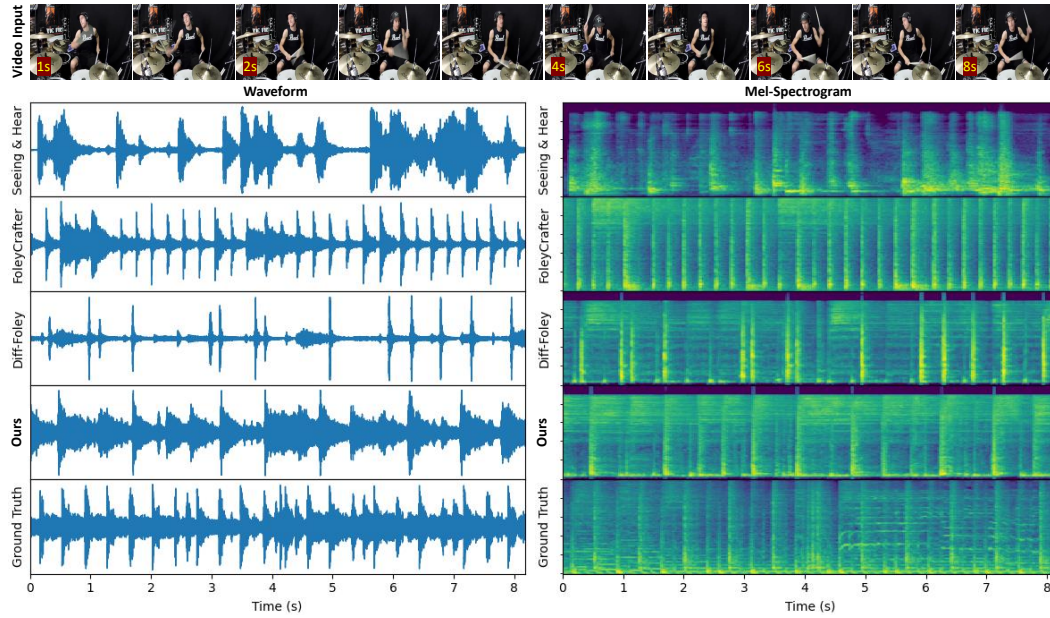


Figure 12: **The video of a guy playing drum by tool.** Our best model (MDSGen-B) generated a sound that is closer to GT compared to existing approaches. We refer the reader to the listen file provided in the supplementary for comparison. File “-Qowmc0P9ic_000034.wav”.

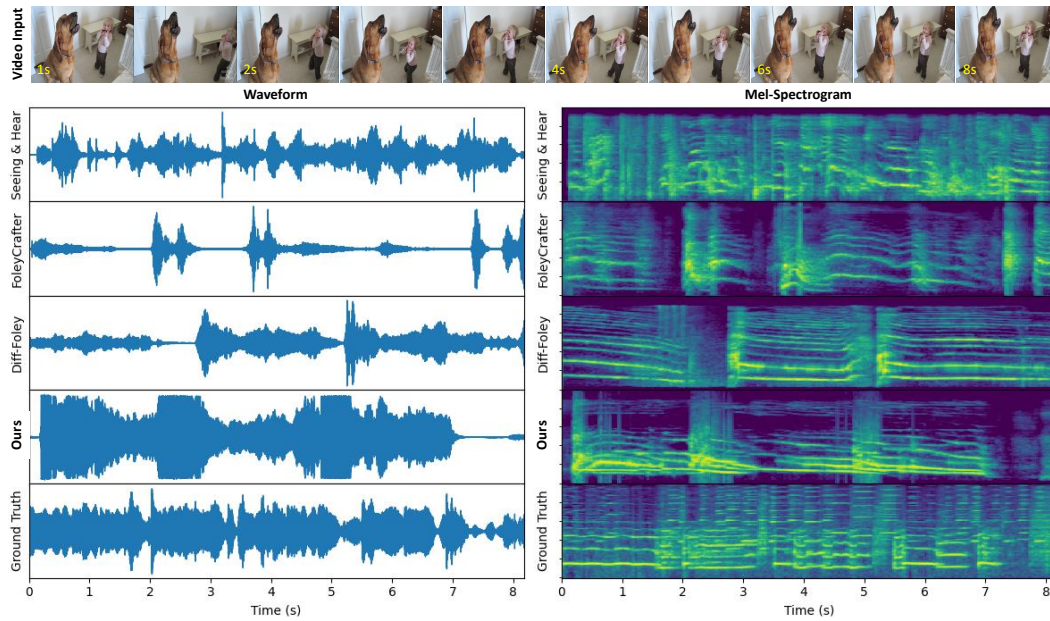


Figure 13: **The video of a dog looks like howling.** Our best model (MDSGen-B) generated a sound closer to GT than existing approaches. We refer the reader to the listen file provided in the supplementary for comparison. File “2vYkvwD-fkc_000010.wav”.

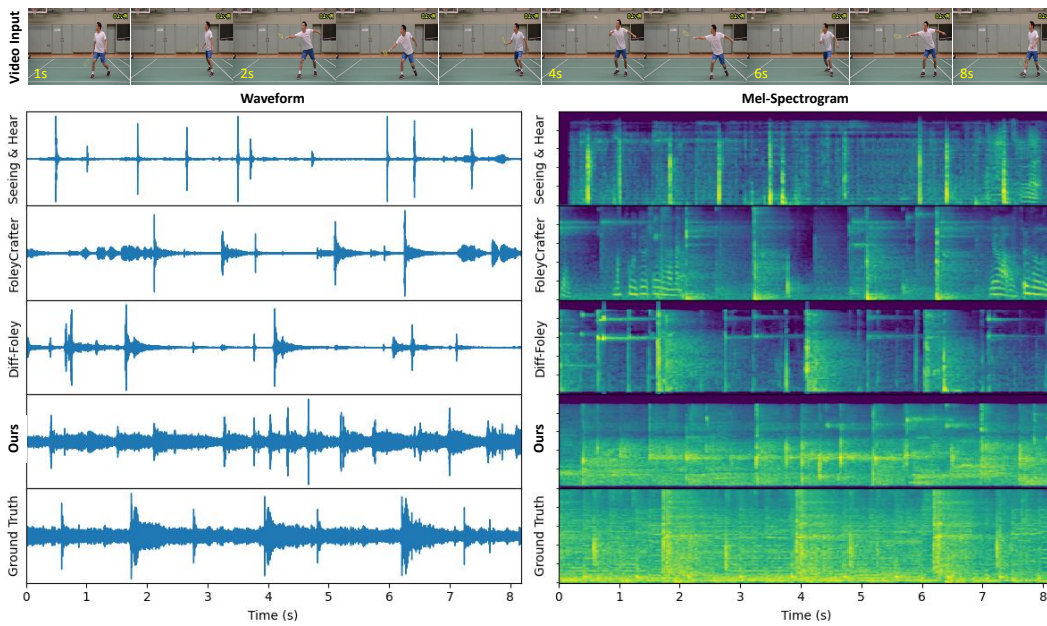


Figure 14: **The video of a guy playing badminton.** Our best model (MDSGen-B) generated a sound that is closer to GT compared to existing approaches. We refer the reader to the listen file provided in the supplementary for comparison. File “-miI_C3At4Y_000104.wav”.

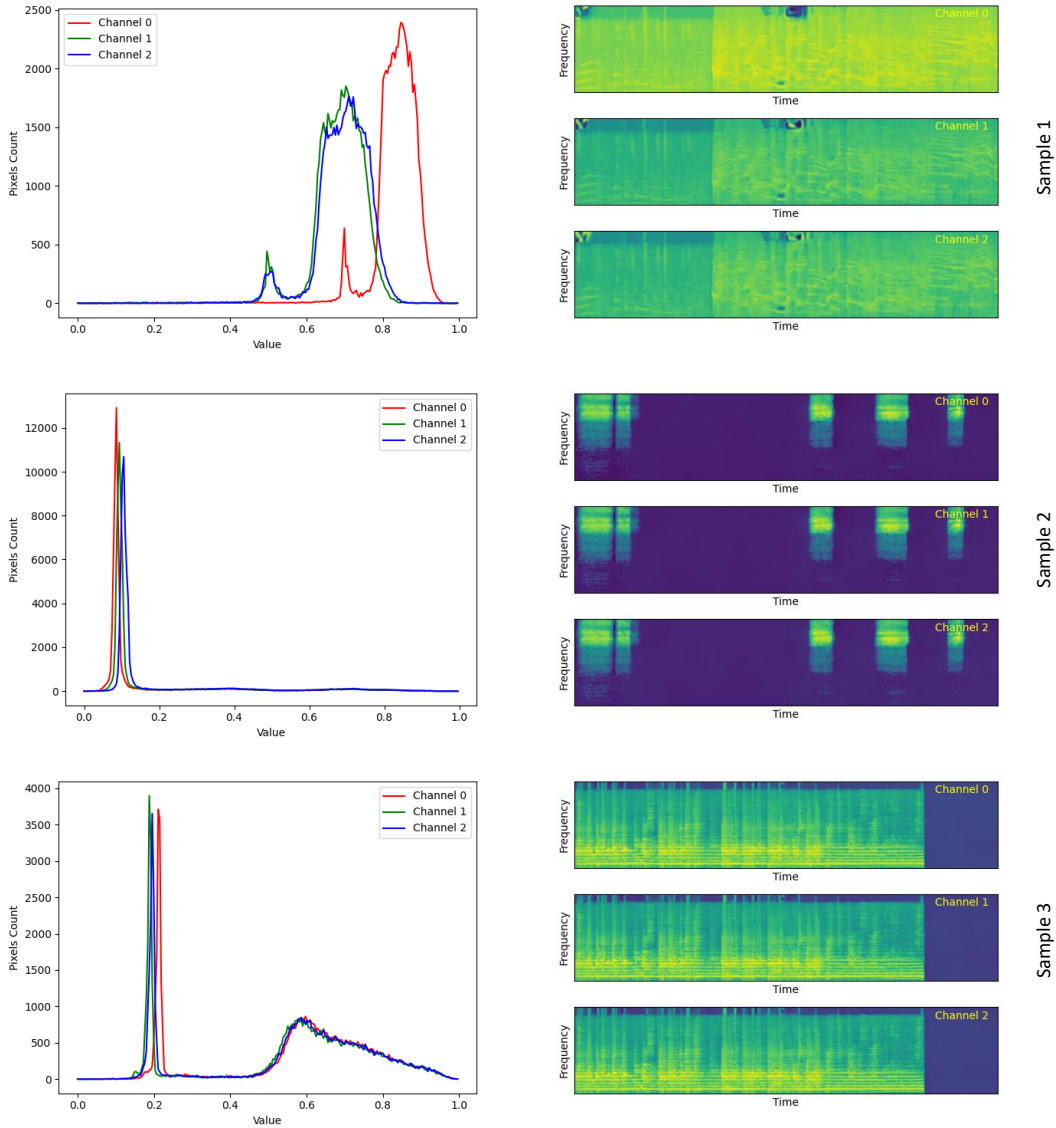


Figure 15: **RGB distribution for Mel-Spectrogram.** We provide more evidential samples that the output of the VAE in the test set yields different characteristics for three channels even though these differences are imperceptible to the human eye (right figures). Interestingly, we find that the first channel (R) always has some different patterns compared to the remained channels (I).

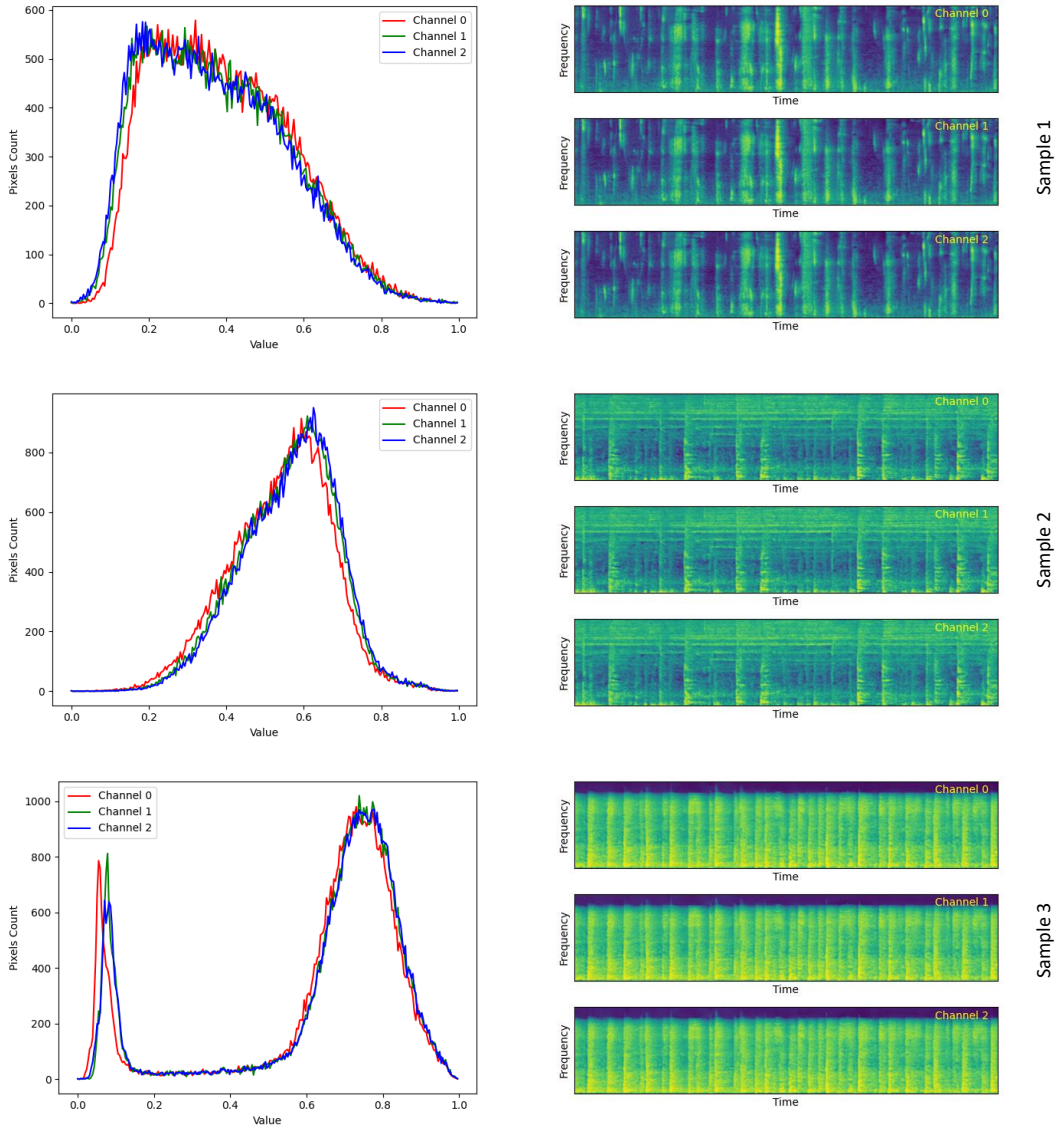


Figure 16: **RGB distribution for Mel-Spectrogram.** We provide more evidential samples that the output of the VAE in the test set yields different characteristics for three channels even though these differences are imperceptible to the human eye (right figures). Interestingly, we find that the first channel (R) always has some different patterns compared to the remained channels (2).